

인터리브드 토템폴 입력단 구조를 갖는 1단 방식과 2단 방식 OBC의 안정도 비교

타반민쑹, 서재희, 최세완
서울과학기술대학교

Stability comparison of Single-Stage vs. Two-Stage OBC with Interleaved totem-pole front-end

Van Minh Thong Ta, Jeahee Seo and Sewan Choi

Department of Electrical and Computer Engineering, Seoul National University of Science and Technology

ABSTRACT

This paper conducts an analysis of the stability of a single-phase OBC system utilizing the input impedance interaction concept. The stability between single-stage (SS) OBC and conventional interleaved totem-pole PFC is compared with considering the EMI filter and the uncertainty of grid impedance. This research investigates the impact of large grid impedance on understanding the origins of oscillation and instability in interleaved totem-pole-based OBCs. The analysis results indicate that the resonant frequency of SS is approximately ten times higher than that of conventional PFC, implying greater resilient to disturbances from the outer loop control.

1. Introduction

According to a maintenance report on OBCs, variations in grid impedance can lead to unexpected oscillations in the input current, potentially triggering the fault protection mechanism of the OBC. This paper investigates the origin of this phenomenon using the impedance interaction concept in [1]. To obtain the input impedance (Z_{IC}) of each topology in Fig. 1, a different small-signal modelling methods are required. Traditional modelling method (state space averaging) in [2] is applied for conventional PFC modelling. Because of the leakage current of SS couldn't be averaged by traditional method so generalized average modelling (GAM) method in [3] is used to model the SS.

2. Input impedance modelling of SS & conventional PFC

2.1 Open-loop input impedance modelling of SS

Traditionally, the input impedance is derived from the small-signal equivalent circuit as described in [2]. However, in this section, the input impedance is formulated based on the large-signal model. Because of the SS modulation fixing the primary side duty cycle at 0.5, the input current (i_{ic}) becomes independent of the control variable in terms of small-signal. The equivalent resistor ($R_{ac} = V_g^2/P$) models the power transfer amount and is represented in parallel with Z_{IC} as shown in Fig. 2(a) The general form of input impedance in frequency domain is:

$$Z_{IC}^l(s) = \frac{1}{R_{ac}} \frac{(2L_g C_{cc} s^2 + 2C_{cc}(R_{Lg} + 2R_{ac})s + 1)}{(2L_g C_{cc} s^2 + 2C_{cc} R_{Lg} s + 1)} \quad (1)$$

Fig. 2(b) illustrates the impedance response results under no-load and rated power conditions. In the low-frequency region, the magnitude of impedance is determined by the equivalent resistor. The self-resonant frequency of SS is determined by $f_r = 1/2\pi\sqrt{2L_g C_{cc}}$.

2.2 Input impedance modelling of conventional PFC

After applying the small-signal modelling to the conventional PFC, the AC equivalent circuit is derived as in Fig. 3. There are two kinds of input impedance. The first one is considered as the open loop input impedance and defined like:

$$Z_D(s) = Z_I(s)|_{\hat{a}(s)=0} \quad (2)$$

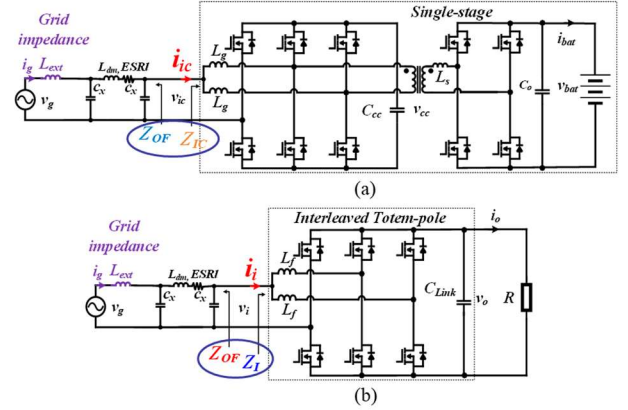


Fig. 1 System definition to analyze the input impedance interaction including EMI filter and grid impedance for (a) Single-stage AC-DC, (b) conventional interleaved totem-pole PFC.

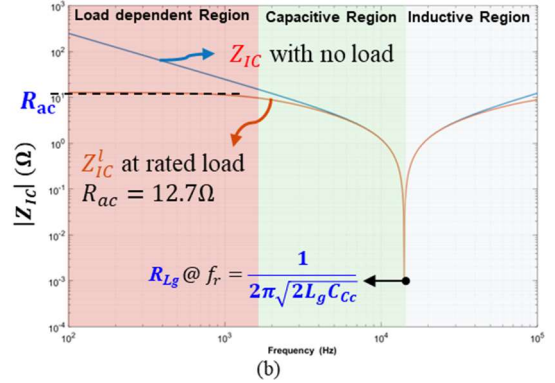
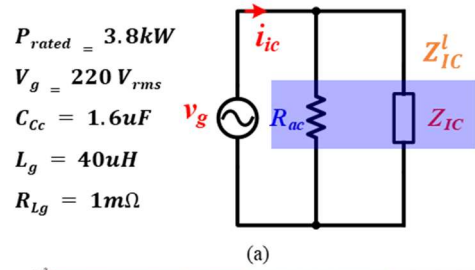


Fig. 2 The open-loop impedance modelling of SS (a) The simple equivalent circuit seen from input side (b) The magnitude responds of open-loop input impedance.

The second impedance is double null injection impedance:

$$Z_N(s) = Z_I(s)|_{\hat{v}_o(s)=0} \quad (3)$$

Both impedances could be obtained by nullifying the respected small signal in the equivalent circuit Fig. 3. Based on the input impedance results shown in Fig. 4, Z_D exhibits behavior like a CL resonant network, while Z_N mainly depend on the load (R) and nominal duty (D) of conventional PFC.

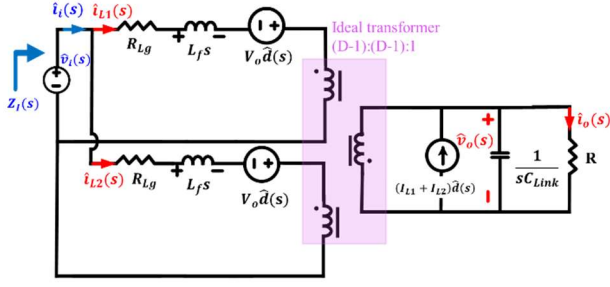


Fig. 3 Small-signal equivalent circuit of conventional PFC

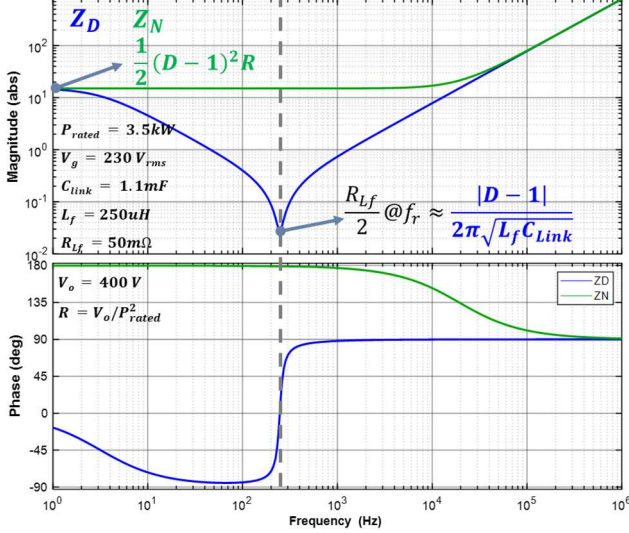


Fig. 4 The characteristic of open loop $Z_D(s)$ and null double injection $Z_N(s)$ input impedance of conventional PFC

2.3 Comparing the input impedance of two topologies.

One common characteristic shared by these two impedances is that they both represent the impedance observed from the input side. However, from the concept to result, there are differences in input impedance between two topologies. Firstly, the input impedance (Z_{IC}) of SS can be derived from the large-signal model, which involves fewer derivation steps compared to the conventional approach. The input impedance of SS can be represented by a single impedance (Z_{IC}^l). In contrast, the comprehensive characteristics of conventional PFC impedance require the use of both Z_D and Z_N . Furthermore, in one grid cycle, Z_{IC}^l don't change but Z_D and Z_N change according to the grid voltage. Lastly, the self-resonant frequency (f_r) of conventional PFC is much lower than SS because the input inductance and link capacitance are significantly larger than clamping capacitance and grid inductance of SS.

3. Closed-loop input impedance modelling & Stability comparison

3.1 Closed-loop input impedance modelling of SS & Minor loop gain concept.

In the closed-loop control structure depicted in Fig. 5, the closed-loop impedance is established by nulling the reference signal.

$$Z_{ic}^c(s) = \tilde{v}_{ic} / \tilde{i}_{ic}|_{\tilde{v}_{ic,d}=0} = Z_{ic}^{ol}(s)(1 + T(s)) \quad (4)$$

where $T(s) = G_{pi}(s)G_{i\phi}(s)$ is the loop gain transfer function of the current loop control. $G_{pi}(s)$ and $G_{i\phi}(s)$ represent the transfer functions of the PI regulator and the control-to-input, respectively.

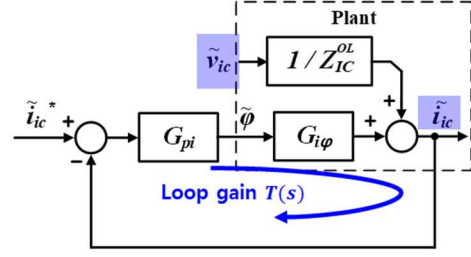


Fig. 5 Closed-loop control structure of SS in term of small-signal.

In the closed-loop system including EMI filter and grid impedance, the minor loop gain concept is defined to examine the system's stability as follows:

$$T_m(s) = Z_{OF}(s)/Z_{IC}^c(s) \quad (5)$$

The results shown in Fig. 6 depict the predicted resonant points of SS from the analysis result. The phase margin (PM) of each resonant point is described in the phase respond graph. The point of minimum phase margin (PM) is most likely to be the cause of instability in this system. Fig. 7 shows the simulation result of the SS's input current. The oscillation frequency in the grid current closely matches with the second intersection point of the frequency domain analysis. This provides validation for the accuracy of the single-stage model and analysis method.

3.2 Closed-loop input impedance modelling of conventional PFC

The closed-loop impedance concept of conventional topology, which could be found in [2], is expressed as:

$$\frac{1}{Z_i(s)} = \frac{1}{Z_N(s)} \frac{T(s)}{1 + T(s)} + \frac{1}{Z_D(s)} \frac{1}{1 + T(s)} \quad (6)$$

where $T(s) = G_{pi}(s)G_{id}(s)$ in this case is the loop gain transfer function of control loop.

The similar minor loop gain (T_m) is also applied to investigate the conventional PFC's system stability under the existing of extra element.

The minor loop's modelling results of conventional PFC is depicted in Fig. 8. There are also two resonant points in this system. These points are caused by the intersection between the closed loop input impedance ($Z_i(s)$) and the output impedance of EMI filter ($Z_{OF}(s)$). The first point is more critical, because its PM is the smallest one. The time-domain simulation depicted in Fig. 9 also illustrate a low frequency resonance occurring in the grid current. By applying the analysis sequence to the conventional PFC, the modeling method can accurately predict the resonant frequency.

3.3 Stability comparison between two topologies by minor loop gain concept.

Based on the modeling and simulation results in Fig. 6-9 of the two systems, the SS topology demonstrates better stability in terms of disturbance immunity. Since the first resonant point in Fig. 8 of the conventional PFC occurs in the low-frequency region, it may be disturbed by the other control loop such as outer voltage control loop, PLL control loop, etc. Furthermore, the EMI filter is unable to attenuate this low-frequency resonance. Secondly, this resonant frequency significantly depends on grid impedance; specifically, larger grid impedance results in a lower resonant frequency, which can exacerbate THD. In contrast, the second resonant point of SS in Fig. 6 system occur in high frequency region that is independent of grid impedance. Which mean that the SS's oscillation frequency can be controlled by modifying EMI filter or passive components of SS.

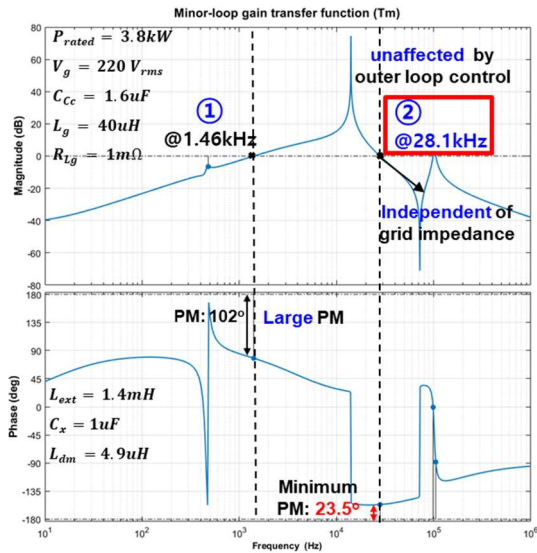


Fig. 6 The magnitude and phase response of SS's minor loop gain under the given grid impedance ($L_{ext} = 1.4mH$).

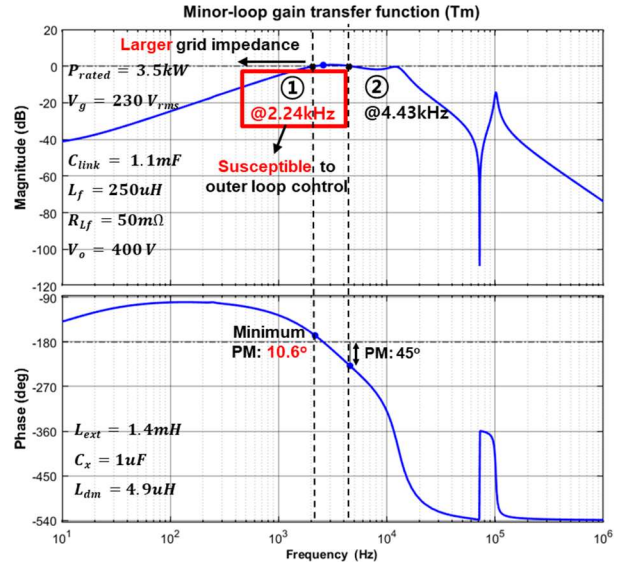


Fig. 8 The magnitude and frequency response of conventional PFC's minor loop gain under the given grid impedance ($L_{ext} = 1.4mH$).

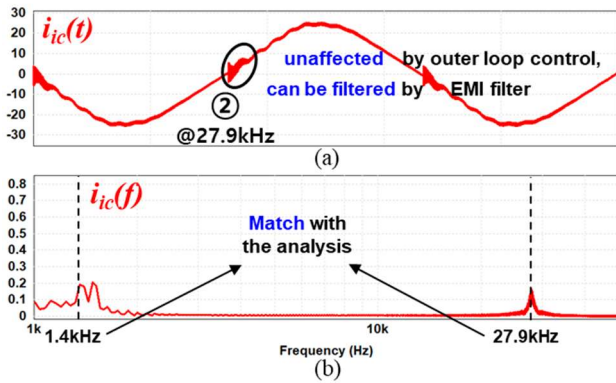


Fig. 7 Simulation result of SS with $L_{ext} = 1.4mH$ (a) time domain waveform of input current (b) frequency spectrum of input current with the oscillation caused by the large grid impedance.

4. Conclusions

From the small-signal modelling method, the paper has provided the accurate analysis sequence to investigate the system stability in the presence of extra elements at the front end of the converter. This method can predict the resonant frequency, assisting control designers in avoiding these critical points. A case comparison between two OBCs is studied to verify the analysis method and investigate the oscillation in each system. In conclusion, the inner current loop of the SS OBC demonstrates greater stability, as its resonant frequency is not influenced by external conditions. The conclusion drawn from analysis results match with the observation of maintenance technicians.

본 과제(결과물)은 교육부와 한국연구재단의 재원으로 지원을 받아 수행된 3단계 산학연협력 선도대학 육성사업 (LINC 3.0)의 연구 결과입니다.

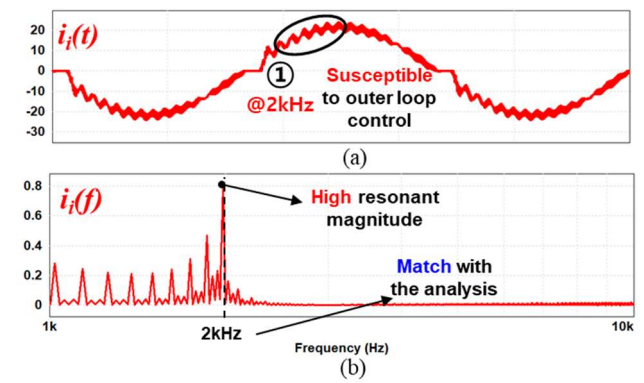


Fig. 9 Simulation result of conventional PFC with $L_{ext} = 1.4mH$ (a) time domain waveform of input current (b) frequency spectrum of input current with the oscillation caused by the large grid impedance.

References

- [1] F. Feng, J. Fang, U. Manandhar, H. B. Gooi, and P. Xie, "Impedance-Based Stability Analysis of DAB Converters With Single-, Double-, or Cooperative Triple-Phase-Shift Modulations and Input LC Filter," *Front Energy Res*, vol. 10, Apr. 2022, doi: 10.3389/fenrg.2022.874477.
- [2] R. W. Erickson and D. Maksimovic, "Fundamentals of Power Electronics SECOND EDITION," *Springer*, pp. 187–406, 2001, doi: 10.1007/978-0-306-48048-5.
- [3] H. Qin and J. W. Kimball, "Generalized average modeling of dual active bridge DC-DC converter," *IEEE Trans Power Electron*, vol. 27, no. 4, pp. 2078–2084, 2012, doi: 10.1109/TPEL.2011.2165734.